Tapered Bragg reflection waveguide edge emitting lasers with near circular twin-beam emission

Ye Yang (杨 晔), Cunzhu Tong (佟存柱)*, Lijie Wang (汪丽杰), Yugang Zeng (曾玉刚), Junsheng Cao (曹军胜), Biao Wang (王 彪), and Lijun Wang (王立军)

State Key laboratory of Luminescence and Applications, Changchun Institute of Optics, Fine Mechanics and Physics, Chinese Academy of Sciences, Changchun 130033, China

**Corresponding author: tongcz@ciomp.ac.cn*

Received August 3, 2013; accepted September 16, 2013; posted online November 4, 2013

An edge emitting laser with two symmetrical near-circular spots located far field (FF) is demonstrated using tapered double-sided Bragg reflection waveguides (BRWs). The BRWs consist of six pairs of top p-type and bottom n-type $Al_{0.1}$ $Ga_{0.9}$ As/$Al_{0.3}$ $Ga_{0.7}$As Bragg reflectors with a period thickness of 850 nm. The device has a 4° tapered angle configuration and exhibits two stable circular beams with a separation angle of 52°. Typical FF angles of 5.87° and 7.8° in the lateral and vertical directions, respectively, are achieved. The lateral FF angle in the ridged section is independent of the injection current (>0.8 A) because of narrow ridge (∼10 μm) confinement. By contrast, the FF angle in the tapered section shows an increase rate of 1.2–1.66°/A. The periodic modulation of the lasing wavelength is observed to be sensitive to self-heating effects.

OCIS codes: 140.5960, 230.1480, 140.3295, 230.7370.
doi: 10.3788/COL201311.121401.

Laser diodes have been widely used in many fields because of their small volume, high electrical drive, high efficiency, and ability to achieve high power densities. One of the most important characteristic parameters of a laser diode that directly affects its realistic applications is the far-field (FF) profile of the output beam. For instance, for the pumping application of solid-state lasers, a narrow single beam with low astigmatism is desired[1]. By contrast, an output of twin beams is expected in applications such as high-speed printing[2,3], high-precision laser detection[4,5], and high-quality laser processing[6]. Hence, controlling the FF behavior of laser diodes has become increasingly important due to the requirements of realistic applications.

Many approaches have been proposed and demonstrated to develop twin-beam lasers; these approaches include coupling of beams from two individual lasers using an optical fiber array or beam-combiner, splitting of one incident beam into two beams using a diffraction grating, and application of a polarization prism, non-degenerate optical parametric oscillator[7], external feedback[8], photonic crystal waveguide[9], surface plasmon[10], and so on. However, these approaches are either limited by complexities in optical alignment and non-compact size or by serious lateral instabilities[11,12]. Thus, natural emitting lasers with two symmetrical and high-quality beams are expected to be of great demand.

In this letter, we experimentally demonstrate a twin beam laser with high beam quality using dual-sided Bragg reflection waveguides (BRWs) and a tapered structure. Application of the tapered waveguide improves the beam quality of the laser and allows us to study the influence of waveguide width on the FF profile base on the same device. The proposed approach allows beam position and beam symmetry control by the design of the waveguide, and all of the necessary components can be integrated on a single chip. Comparisons of output properties, such as power and lasing spectra, between the tapered and ridge waveguide (RW) sections are presented. The current dependence of the FF behavior is also investigated and discussed.

Figure 1(a) shows a schematic of the designed dual-side BRW laser (BRL), which consists of a quantum well (QW) gain medium located at the center of a core layer and p-type top and n-type bottom BRWs. We designed

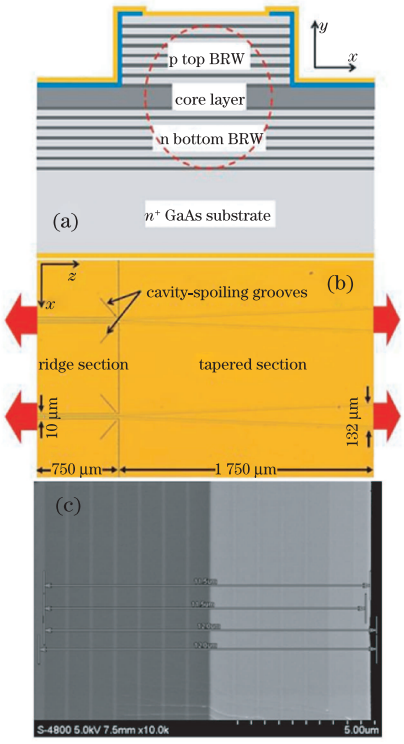

Fig. 1. (Color online) Tapered Bragg reflection waveguide laser (BRL). (a) Schematic of the BRL structure; (b) top-view of the device; (c) SEM image of the expitaxial structure of the laser.

the refractive indices of the BRWs to generate a near-field (NF) profile with discrete peaks, and the peak intensities decrease from the center to either side in exponential evanescence to present a two-lobed FF pattern. The mechanism behind this setup was presented in detail in our previous study[13]and can be simplified as follows. Because light propagation occurs as a zigzag wave, the optical wave emitted from the cavity is angled toward the normal plane of the cavity facet. If the tilt angle incident on the facet is lower than the angle of the total internal reflection at the semiconductor-air interface, the FF pattern is composed of two lobes[13–15]. To reduce the divergence of two emission beams, we selected six pairs of $Al_{0.1}Ga_{0.9}As/Al_{0.3}Ga_{0.7}As$ Bragg reflectors with a pair thickness of 850 nm. The total thickness of the BRWs was over 10 μm. The low index difference in the reflector material allowed the electromagnetic fields to extend to the whole cavity, which reduces the FF angle of the emission beams to within several degrees of those reported in the theoretical analysis provided in Ref. [13].

To further improve the beam quality and emission power of our system, we designed a tapered BRL. Figure 1(b) shows the top-view of the device obtained. The structure consists of a tapered angle of 4° together with a tapered section length of 1.75 mm, which produces an emitting aperture of about 132 μm in width. The length of the ridge section is 750 μm and its width is 10 μm, resulting in a total device length of 2.5 mm. Cavity-spoiling grooves were symmetrically set on both sides of the ridge to prevent higher-order mode oscillation[16].

The epitaxial structure of the device was grown on (100)-oriented, n^+ GaAs using metal-organic chemical vapor deposition (AIXTRON 200/4, Aixtron, Korea). Two 6-nm $In_{0.2}Ga_{0.8}As$ QWs were separated by 10-nm GaAs located at the center of the 1.5-μm $Al_{0.3}Ga_{0.7}As$ core layer and then sandwiched between the top and bottom BRWs. The total thickness of the epitaxial layer was 12.7 μm. Figure 1(c) shows an image of the epitaxial structure obtained by scanning electron microscopy (SEM); this image clearly reveals the top and bottom Bragg reflectors. The devices were fabricated by standard compound semiconductor fabrication techniques. The RW and tapered sections were processed by wet chemical etching followed by a lift-off step. Tri-layer Ti/Pt/Au and Au/Ge/Ni contacts were respectively deposited on the p-side and n-side of the device as electrodes. To investigate the output properties of the two facets in the tapered BRL, laser chips were uncoated and mounted p-side down on copper mounts without soldering and packaging for measurement.

Figure 2 shows the light–current–voltage (L–I-V) characteristics of the tapered and RW facets of the BRL under pulse operation (pulse width=100 μs, repetition rate=1 kHz) at room temperature (RT). The output power from the tapered facet reaches 80 mW, and its slope efficiency is 0.1 W/A. For the RW facet, the highest light power obtained is around 66 mW, and obvious saturation is observed when the injection current exceeds 1.2 A. In tapered semiconductor lasers, the majority of the gain is provided by forward propagation in the tapered section, while beam amplification in the RW section is limited by losses caused by filtering and reflection or absorption in the beam spoilers[17]. Differences in injection area and

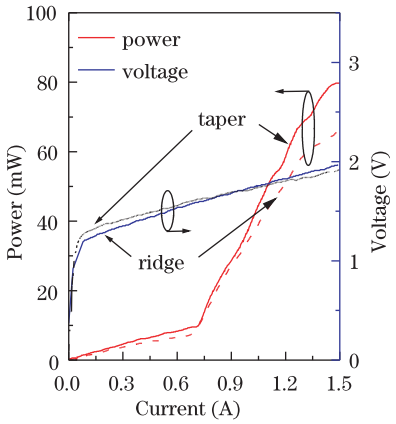

Fig. 2. (Color online) Power-current and voltage-current characteristics of the tapered facet and ridge facet of the tapered BRL at room temperature.

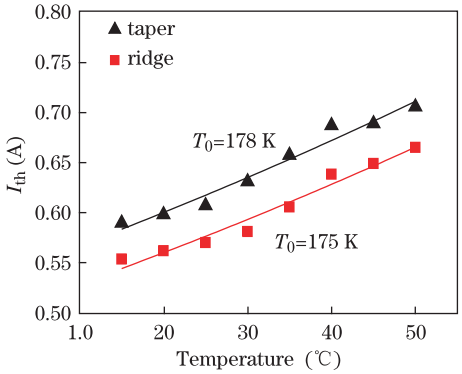

Fig. 3. (Color online) Temperature dependence of the threshold currents of the tapered and RW facets of the tapered BRL.

heat accumulation also contribute to variations in the threshold and output performances of the tapered and RW sections.

The threshold currents of the tapered facet of the BRL at different temperatures are shown in Fig. 3; significant differences in threshold current are observed under lasing from the tapered (triangles) and RW (squares) facets. The threshold current at the tapered facet varies from 0.59 to 0.70 A as the temperature increases from 15 to 50 °C and is almost 40 mA higher than that at the RW facet. The characteristic temperatures (T_0) of the tapered and RW facets are 178 and 175 K, respectively. These findings show that self-heating effects in the tapered section are slightly better than those in the RW section. Thus, the high threshold current in the tapered section is mainly due to its large injection area.

The two-dimensional (2D) FF behavior of the tapered BRL is presented in Fig. 4(a). Two pronounced lobes in the vertical direction, which remain stable over the entire range of tested currents, are observed. The lobes are symmetric and nearly circular and become brighter with increasing injection current. The spots from the tapered facet show a small extension in the transverse direction when the current is above 1 A; this phenomenon is due to current diffusion through the large-sized tapered section. By contrast, the RW section reveals clean spots without extensions. Detailed FF profiles in the vertical direction are shown in Figs. 4(b) and (c), from which we

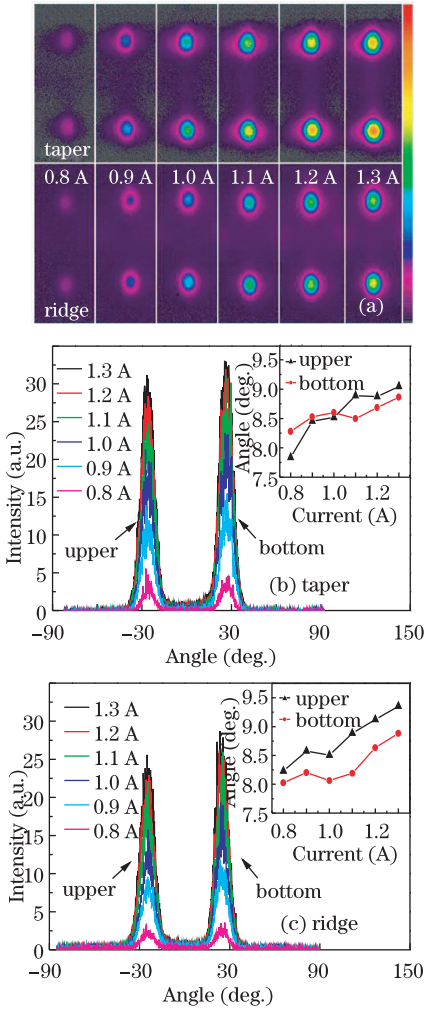

Fig. 4. (Color online) (a) Two-dimensional FF patterns measured from the tapered and RW facets of the tapered BRL at different currents above the threshold. Vertical FF profiles of the (b) tapered and (c) RW facets of the tapered BRL are also obtained. The insets show the FWHM of the upper and bottom lobes in the vertical direction.

can determine the symmetry of the lasing twin spots. In the tapered section in Fig. 4(b), the centers of the two lobes are located at –26.1° and 26.4°.

The peak intensity of the bottom lobe is higher than that of the top lobe, which results from higher leak losses in the high-index substrate. As shown in the inset in Fig. 4(b), the full-width at half maximum (FWHM) values of the front-vertical FF profile in the upper and bottom lobes are 7.8° and 8.3°, respectively, at 0.8-A current and increase by about 1° as the current increases to 1.3 A. The corresponding current dependence rates are 1.6 and 1.2 °/A, respectively. The FF angle is defined as the FWHM of the FF profile; thus, in the next sections, the FF angle is used to describe the FF properties.

Figure 4(c) shows the corresponding FF profiles obtained from the RW section. The inset in Fig. 4(c) shows that the FF angle of the upper lobe expands from 8.2° to 9.3° as the current increases from 0.8 to 1.3 A, i.e., the FF expansion attributed to the diffusion of the injected current is about 2.2 °/A. By contrast, the FF angle changes at a rate of 1.8 °/A for the bottom lobe. While the characteristics of vertical FF are determined by BRWs, the tapered section obviously presents better heat dissipating capability than the RW section so that higher intensities and the slight lower vertical divergence angles are realized. Moreover, in both tapered and RW sections, increases in the injection current result the extension of the optical field toward the vertical direction of the device as well as increases in the FF angle. Variations are more significant in the RW section than that in the tapered section.

Figure 5 shows the lateral FF angles of the upper and bottom lobes of the tapered and RW facets of the tapered BRL as measured under different injected currents. The FF angles of the upper and bottom lobes in the tapered section are 5.87° and 5.83°, respectively, at 0.8-A current and increase to 6.7° at 1.3 A. The expansion rate of the current is about 1.66 °/A, which is nearly identical to the rate in the vertical direction, as shown in Figs. 4(b) and (c). By contrast, the lateral FF angle of the RW section is about 5.7° and remains almost unchanged with variations in injected current. These results reveal that current diffusion in the transverse direction reaches the limit for a 10-μm wide ridge when the injection current is above 0.8 A. In the tapered section, current diffusion in the lateral direction results in an increase in the FF angle at a rate of 2 °/A.

The inset in Fig. 5 shows that the lateral FF presents a Gaussian profile. Two main mechanisms are known to limit the beam quality of tapered lasers: poor modal filtering in the RW section and beam self-focusing in the tapered section at high power levels[17]. Modal filtering may be improved significantly by the inclusion of beam spoilers such that the RW section of tapered BRLs presents stable basic-mode emission. Beam self-focusing is induced by the parasitic carrier-induced waveguide at the beam center, which is caused by the spatial hole burning effect. Thus, the beam of the tapered section deteriorates with increases in current and power.

A spectral map plotted on a log scale measured for numerous currents with a step size of 10 mA is depicted in Fig. 6. The tapered facet exhibits a narrow spectrum with a FWHM of 1 nm and fairly pronounced modulation with a period of approximately 3.7 nm. The lasing wavelength begins at about 994.2 nm at 0.71 A and shifts slowly to longer wavelengths with increases in the pump current. A second peak wavelength of 997.9 nm appears at 0.82 A and becomes the major mode operating in the

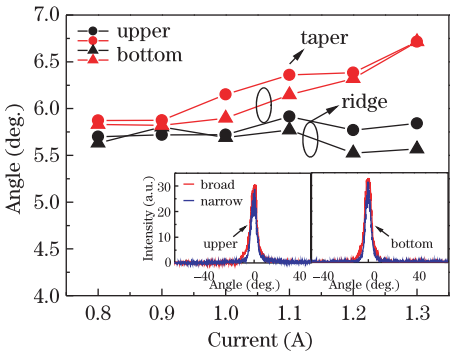

Fig. 5. (Color online) Lateral FF angles obtained from the tapered and RW facets of the tapered BRL at different input currents. Inset: Comparison of the lateral FF profiles of the tapered and RW facets.

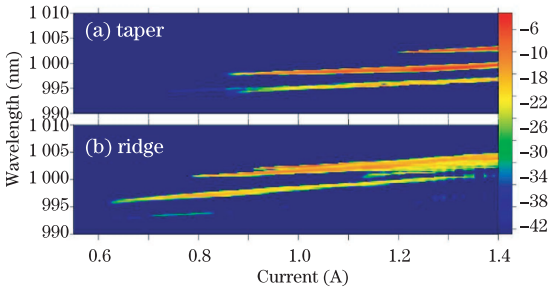

Fig. 6. (Color online) Color-scale mapping of the spectrum versus injection current for (a) the front facet of the tapered section and (b) the back facet of the RW section of the tapered BRL.

laser. At this point, the spectral intensity gradually increases with the current. At 1.2 A, a third peak wavelength of 1002.2 nm appears and three peaks may be observed simultaneously. This periodic wavelength originates from self-heating of the device, which causes a significant thermal shift in the gain spectrum of the QWs and small variations in the BRW reflectivity according to the changes in the refractive index. We attribute the special spectral characteristics of BRLs to the additional feedback mechanism originating from distributed reflections in the BRWs.

The spectrum of the RW facet also displays periodic modulation. However, the spectrum width of this facet broadens to nearly 3 nm at higher currents (1.2–1.4 A); this broadening is attributed to the poor heat dissipating capability of the narrow ridge and leads to overlapping of the contiguous lasing peaks. Periodic separation of the lasing wavelength may inspire new applications in the fields of optical frequency combs and broad-spectrum mode-locked lasers, among others.

In conclusion, a tapered BRL with two near-circular FF beams is demonstrated, and the output properties, FF distribution, and spectral properties of its tapered and RW sections are studied. Typical FF angles of 5.87° and 7.8° are respectively achieved in the lateral and vertical directions. The tapered section presents a current-sensitive FF angle that increases at a rate of 1.66 °/A in the lateral direction and 1.2–1.6 °/A in the vertical direction. The lateral FF angle in the RW section, on the other hand, is limited to about 5.7° because of the narrow ridge (width, 10 μm). We believe that these results will contribute to the future development of high-performance compact twin-beam laser sources.

This work was supported by the National Natural Science Foundation of China (Nos. 61076064 and 61176046), the China Postdoctoral Science Foundation (No. 2011M500621), and the Open Project of the State Key Lab on Integrated Optoelectronics (No. 2011KFB006).

References

1. J. Zhang, L. Liu, W. Chen, A. Liu, W. Zhou, and W. Zheng, Chin. Opt. Lett. **10,** 061401 (2012).
2. K. Kataoka, Opt. Rev. **15,** 196 (2008).
3. A. Arimoto, S. Saitoh, T. Mochizuki, Y. Kikuchi, and K. Hatazawa, Appl. Opt. **26,** 2554 (1987).
4. A. Heidmann, R. J. Horowicz, S. Reynaud, E. Giacobino, C. Fabre, and G. Camy, Phys. Rev. Lett. **59,** 2555 (1987).
5. N. T. K. Thanh, J. H. Rees, and Z. Rosenzweig, Anal. Bioanal. Chem. **374,** 1174 (2002).
6. J. Xie, Weld. J. **81,** 223s (2002).
7. K. Hayasaka, Y. Zhang, and K. Kasai, Opt. Lett. **29,** 1665 (2004).
8. M. Chi, N. S. Bøgh, B. Thestrup, and P. M. Petersen, Appl. Phys. Lett. **85,** 1107 (2004).
9. W. Jia, J. Deng, H. Wu, X. Li, and A. J. Danner, Opt. Lett. **36,** 4077 (2011).
10. X. Li, Q. Tan, B. Bai, and G. Jin, Chin. Opt. Lett. **10,** 052401 (2012).
11. M. K. Chun, T. L. Whitman, and D. G. Soenksen, Appl. Opt. **26,** 4518 (1987).
12. A. Jechow, M. Lichtner, R. Menzel, M. Radziunas, D. Skoczowsky, and A. G. Vladimirov, Opt. Express **17,** 19599 (2009).
13. L. Wang, Y. Yang, Y. G. Zeng, L. J. Wang, C. Z. Tong, X. N. Shan, H. X. Zhao, R. Wang, and S. F. Yoon, Appl. Phys. B **107,** 809 (2012).
14. V. I. Shveikin, A. P. Bogatov, A. E. Drakin, and Y. V. Kurnyavko, Quantum Electron. **29,** 33 (1999).
15. N. Zareian, P. Abolghasem, and A. S. Helmy, J. Lightwave Technol. **29,** 728 (2011).
16. J. N. Walpole, E. S. Kintzer, S. R. Chinn, C. A. Wang, and L. J. Missaggia, Appl. Phys. Lett. **61,** 740 (1992).
17. L. Borruel, S. Sujecki, J. Wykes, H. Wenzel, E. C. Larkins, and I. Esquivias, in *Proceedings of the 4th International Conference on the Numerical Simulation of Optoelectronic Devices* (*NUSOD*) 9 (2004).